Published in Journal of Optics A: Pure and Applied Optics 6, issue 5, 189-196, 2004
which should be used for any reference to this work

Measuring optical phase singularities at subwavelength resolution

René Dändliker[1], Iwan Märki, Martin Salt and Antonello Nesci[2]

Institute of Microtechnology, University of Neuchatel, Breguet 2, CH-2000 Neuchatel, Switzerland
E-mail: rene.dandliker@unine.ch

Abstract

We will present experimental and theoretical studies of optical fields with subwavelength structures, in particular phase singularities and coherent detection methods with nanometric resolution. An electromagnetic field is characterized by an amplitude, a phase and a polarization state. Therefore, experimental studies require coherent detection methods, which allow one to measure the amplitude and phase of the optical field with subwavelength resolution. We will present two instruments, a heterodyne scanning probe microscope (heterodyne SNOM) and a high resolution interference microscope (HRIM). We will review some earlier work using the heterodyne SNOM, in particular the measurement of phase singularities produced by a 1 μm pitch grating with 10 nm spatial sampling. Using the HRIM we have investigated the intensity and phase distributions (with singularities) in the focal region of microlenses. The measurements are compared with the results calculated by rigorous diffraction theory.

Keywords: scanning optical probe microscopy, interference microscopy, sub-wavelength features, nano-optics, phase measurement, phase singularities, micro-lenses

1. Introduction

Optical fields are characterized by an amplitude, a phase and a polarization state. Coherent light diffracted by microstructures produces subwavelength features and can give birth to phase dislocations, also called phase singularities. Phase singularities are isolated points where the amplitude of the field is zero. In classical microscopy the objects are in general illuminated by incoherent light, and therefore only the intensity is measured. That is probably why historically most investigations (including discussions on resolution, imaging properties etc) are based on the intensity distribution. For phase measurements, coherent illumination and interference of the object wave with a reference wave are needed, like in interference microscopy. In the neighbourhood of phase singularities the phase varies rapidly at a subwavelength scale. To investigate these phase variations and to localize the position of the phase singularities with high precision, we use two different instruments with subwavelength resolution: a heterodyne scanning probe microscope (heterodyne SNOM) [1] and a high resolution interference microscope (HRIM) [2].

In this paper we wish to give a review of some earlier work with the heterodyne SNOM [3] and some new results obtained with the HRIM. We present measurements of phase singularities with 10 nm spatial sampling and compare them with theoretical results obtained from rigorous diffraction calculations. We made measurements of amplitude and phase with the heterodyne SNOM in the optical field diffracted by periodic microstructures, in particular a holographically recorded 1 μm pitch grating. We have also investigated the

[1] http://www-imt.unine.ch
[2] Present address: Nanophotonics and Metrology Laboratory, Swiss Federal Institute of Technology Lausanne (EPFL), CH-1015 Lausanne, Switzerland.

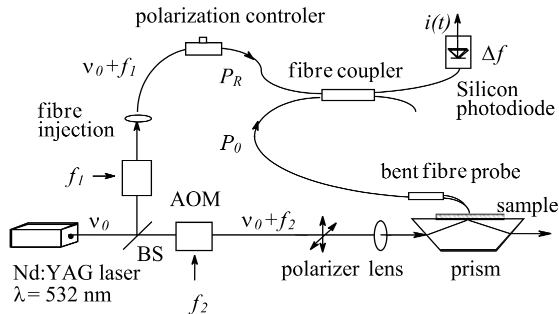

Figure 1. The heterodyne scanning probe microscope [1].

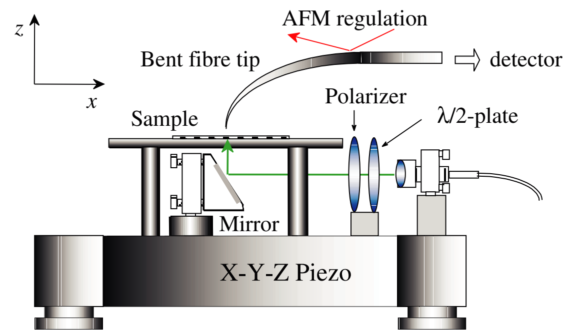

Figure 2. The experimental set-up for the illumination of the sample and the fibre tip probe [3].

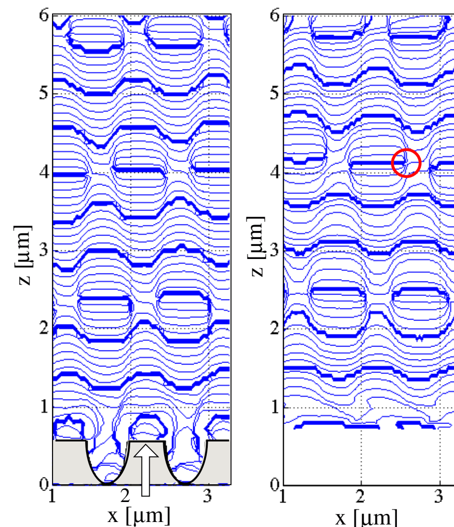

Figure 3. Left: the phase distribution calculated with the Fourier modal method. Right: the measured phase. The circle encloses one phase singularity [3].

3D intensity and phase distributions in the focal region of microlenses using the HRIM. The measurements are compared with the theoretical results obtained with a 2D model.

2. Heterodyne scanning probe microscope (heterodyne SNOM)

We have developed a coherent scanning near-field optical microscope (SNOM) with heterodyne detection for accurate phase measurements [1]. The concept of heterodyne interferometry is introducing a small frequency shift Δf between two interfering beams. Due to this, the interference of the two beams produces an intensity modulation at the beat frequency $\Delta f = f_1 - f_2$, which is then detected. The set-up of the SNOM with heterodyne detection is shown in figure 1.

The laser is a 150 mW frequency doubled Nd:YAG diode-pumped solid-state laser ($\lambda = 532$ nm). After separation by a beam splitter (BS), the object and reference beams are shifted in frequency by two acousto-optic modulators (AOM), driven at $f_1 = 40.07$ MHz and $f_2 = 40.00$ MHz, respectively. On approaching a commercial AFM cantilever fibre probe close to the surface, the field is perturbed, resulting in propagation in the fibre. The reference and object beams are combined in the fibre coupler, producing the beat signal at 70 kHz, detected by a standard silicon photodiode. A polarization controller is used to get maximum interference. During the measurement, the polarization is stable. Using synchronous detection of the heterodyne signal with a lock-in amplifier, we get two electronic output signals from which the amplitude and the phase of the optical field can be deduced. Besides the coherent detection allowing the optical field phase to be determined, we also get an increased dynamic range. This is because the amplitude of the electrical signal is proportional to the amplitude of the optical field, rather than to the intensity. In addition, we can always get shot-noise-limited detection, even with a photodiode, if P_R is chosen to be sufficiently large to overcome the electronic noise.

The illumination system for the samples is shown in figure 2. The illumination system and the sample are mounted on an x–y–z piezoelectric translation stage (100 μm $\times$ 100 μm $\times$ 20 μm range), which allows accurate translation steps (2 nm resolution in the z-direction). The fibre tip is mounted independently of this translation system. The bent tip is used as a conventional AFM (atomic force microscope) cantilever and is brought close to the surface. Once the tip approach has been done, the AFM feedback (contact mode) is switched off and the scan (in XY or XZ planes) is accomplished by the x–y–z stage. Most SNOM measurements are done at constant height (or constant intensity) in the X–Y plane (parallel to the surface) above the samples. However, the optical field diffracted by a structure depends strongly on the z-position, normal to the surface. Therefore, we have performed scans above the structures in the X–Z plane, perpendicular to the surface.

3. Phase singularities generated by a 1 μm grating

The sample is a 1 μm pitch quasi-binary shape grating of about 0.7 μm depth, holographically recorded in photoresist. We use a dielectric fibre tip to collect the field information. The small coupling between the dielectric tip and the dielectric grating gives a negligible contribution to the total electric field. Using the set-up of figure 2, measurements of the TE-mode amplitude and phase in the X–Z plane have been performed. Results of the phase measurements are shown in figure 3 together with the theoretical phase distribution calculated with a Fourier modal method (FMM). The phases in figure 3 are represented by contour plots (isophase lines). The distance between two 'bold' lines is λ (and thus corresponds to 2π). The measured phase distribution shown in the left figure 3 is a zoom into

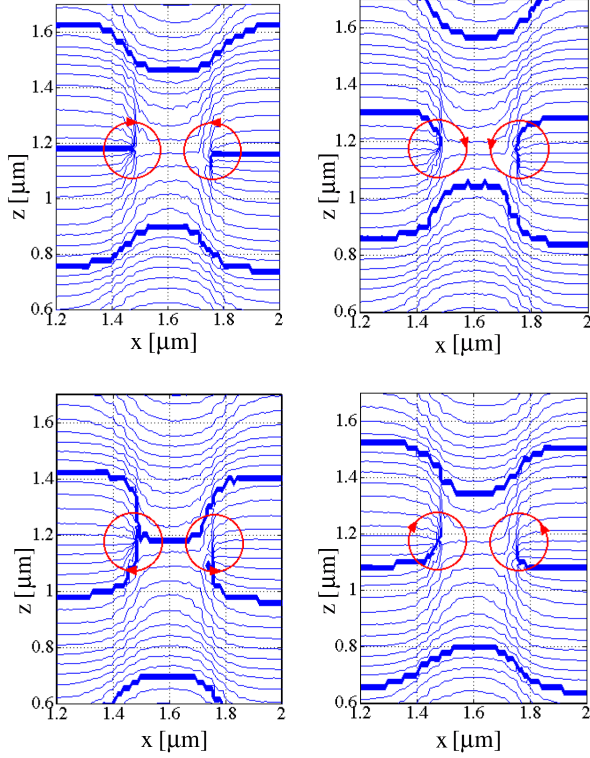

Figure 4. The phase measurement around two adjacent singularities separated by less than 300 nm. The scan step is 10 nm in the x-direction and 20 nm in the z-direction. The additional reference phase increases from left to right in steps of 90°. The opposite sense of rotation indicates the opposite topological charge of the two singularities.

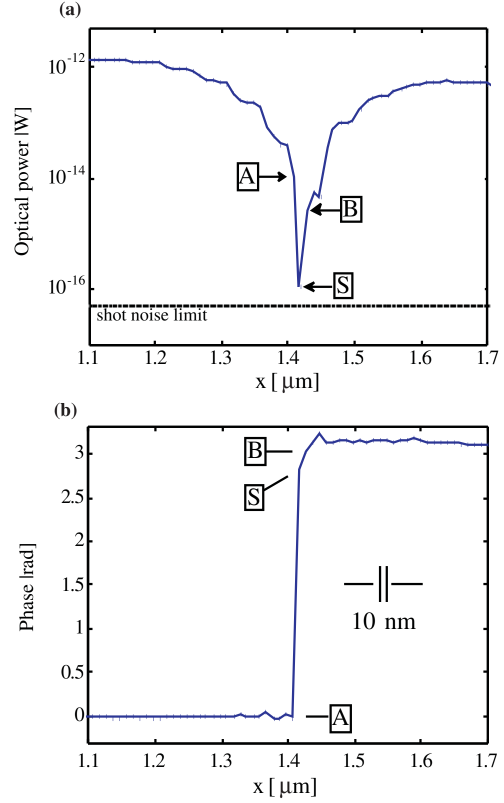

Figure 5. The optical power and phase measured crossing a phase singularity (S). The phase singularity is the special point where (a) the amplitude is zero and (b) the phase jumps by π (with a quasi-infinite slope) [3].

a larger field, which has been acquired by scanning in the x-direction at constant height with a step of $\Delta x = 25$ nm, starting at $z = 10$ μm and moving down in $\Delta z = 50$ nm steps for further x-line scans. The total scan size was $x = 5$ μm by $z = 10$ μm and the number of pixels is 200×200. With an integration time of 30 ms/pixel, the total image was acquired in 20 min. The circle indicates a phase singularity, an isolated point where the amplitude is zero and the phase is not determined [4]. Comparison with the theoretical calculations (right in figure 3) shows a very good agreement, at least for the field measured more than 0.5 μm above the grating.

The evolution of the optical phase in time can be simulated by an additional linearly increasing phase of the reference wave. In figure 4 we present another measurement of the phase around two adjacent singularities using the following approach: the reference phase increases from left to right in steps of 90°. The spatial sampling of the measurements is 10 nm in the x-direction and 20 nm in the z-direction. We observe that the measured phase distribution changes its shape, but the phase singularities do not change their position. As the wave propagates in the z-direction, the phase distribution turns around the two phase singularities in the opposite direction, which means that they have opposite topological charge.

Figure 5 shows another measurement, but similar to a cross-section of figure 4 at $z = 1.18$ μm. On crossing the phase singularity, the amplitude makes a transition through zero (figure 5(a)) and the phase jump is always π (figure 5(b)). In this figure, we demonstrate that, at a phase singularity, the phase is not defined (because the signal vanishes in the noise) and the amplitude is really zero. In fact, we measured the zero amplitude or, more precisely, the zero optical power, down to $P_0 = 10^{-16}$ W (figure 5(a), with the marker 'S'). The theoretical minimum detectable power at 50 Hz bandwidth is $P_{\mathrm{min}} = 2.7 \times 10^{-17}$ W, limited by the shot noise. Thus the detected point is very close to the shot noise. The transition of the phase in figure 5(b) is measured within one step of ± 10 nm. The measured phase jump is as sharp as one step (with a slope of $18°$ nm^{-1}).

From these measurements we see that although the amplitude falls practically down to zero at the singularity, the signal-to-noise ratio around the phase singularity (figure 5(b), markers A and B, separated by 20 nm) is sufficiently large to locate the phase jump with high accuracy. In fact, in figure 5(b), the signal-to-noise ratios at the points A, S and B are $\mathrm{SNR_A} = 26$ dB, $\mathrm{SNR_S} = 6$ dB and $\mathrm{SNR_B} = 21$ dB, respectively, corresponding to the optical powers of $P_{\mathrm{A}} = 10^{-14}$ W, $P_{\mathrm{S}} = 10^{-16}$ W and $P_{\mathrm{B}} = 3 \times 10^{-15}$ W. The resulting standard deviations for the phase measurement are $\delta\varphi_{\mathrm{A}} = 3°$, $\delta\varphi_{\mathrm{S}} = 30°$ and $\delta\varphi_{\mathrm{B}} = 5°$. Although the phase is not well measured at S, the transition is very well localized (within 10–20 nm) by the measurements at points A and B in figure 5(b).

In previous papers we have also discussed the vectorial aspects of the electromagnetic field detection with fibre optical SNOM probes [3, 5]. We did observe some interesting

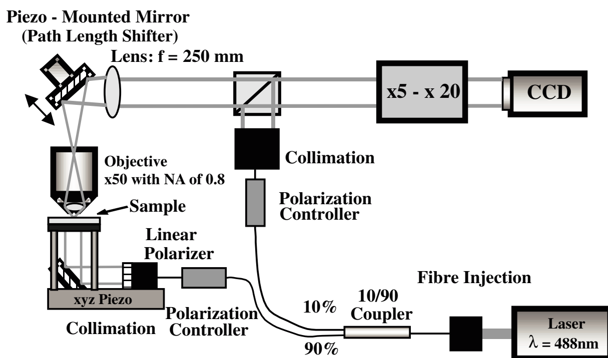

Figure 6. A schematic view of the high resolution interference microscope. The pixel size of the CCD is about 10 μm.

polarization effects for the TM diffraction mode, which has an important longitudinal electric field component in this non-paraxial case, and our conclusion was that the longitudinal component of the electric field contributes nearly as much as the transverse component to the excitation of the propagating mode in the fibre probe.

4. High resolution interference microscope

We have modified a classical interference microscope based on a Mach–Zehnder interferometer by adding a second magnification stage to obtain high spatial accuracy (see figure 6) [2]. The instrument is suitable for studying test structures in transmission. The typical overall magnification of the interference microscope is up to 1000, giving rise to a pixel size in the object field between 10 and 50 nm. The resolution of the far-field measurements is, of course, diffraction limited. The test structures are illuminated by a linearly polarized plane wave of wavelength $\lambda = 488$ nm. A piezo-stage is used for precise z-positioning of the test element. 3D measurements are created via z-stepping of whole x–y areas, read consecutively using an area CCD. Thus, the different sections (x–y, x–z, y–z) can be observed by taking slices through the completed 3D data array. The phase information of the optical field is obtained by a classical five-frame error-compensation algorithm [6]. Varying the phase difference between the two interfering beams in a known manner (phase shifts of $\pi/2$ introduced by a PZT-mounted mirror), five intensity distributions are acquired and the original phase difference between the interfering beams can be calculated. The first studies in the field of high resolution interferometry were carried out by Tychinski [7]. He observed structures of the phase distribution inside a diffraction-limited spot. Convincing explanations of the apparent superresolution phenomenon have been given only recently by Totzeck and Tiziani [8, 9]. With a high resolution interference microscope, phase singularities can be observed [2]. Phase singularities can be observed in both the near and far fields of optical microstructures. The phase jump at singularities is very sharp, which allows the determination of their position with subwavelength accuracy. However, since the electromagnetic field decreases to zero, the detected signal decreases in the vicinity of a singularity and the accurate location of two close singularities is therefore limited by the signal-to-noise ratio.

5. Phase singularities in the focal region of microlenses

Micro-optical elements play an important role in a large range of applications, notably in integrated optical systems. Today's technology allows the realization of a great variety of micro-optical elements, and several simulation methods have been developed in order to model the interaction of light with such optical microstructures [10, 11]. The ability to image and compute the optical field of micro-optical elements allows a better understanding of the optical phenomena that occur. In this paper we discuss the simulation and measurement of the optical field in the focal region of a refractive microlens. Similar studies have already been presented [12–15], however, with limited experimental results. To the best of our knowledge, we present for the first time combined theoretical and three-dimensional experimental investigations. For this purpose, the Fourier modal method (FMM) based on rigorous diffraction theory [16] was applied and, by means of high resolution interference microscopy, the intensity and phase distribution of the optical field generated by a microlens was measured.

A common and well-known method for fabricating refractive microlenses is the resist melting technology or reflow technique [17]. This technology was used to fabricate the microlens arrays discussed in this paper. The investigations presented add more information about the behaviour of the optical field in the focal region of refractive microlenses with a diameter of the order of 30 μm and high numerical apertures (NA $\approx$ 0.4).

On the basis of a standard rigorous diffraction theory, we apply the rigorous eigenmode method (FMM) to the simulation of microlens arrays [16]. The rigorous eigenmode method is applicable to a wide range of periodic profiles but is limited by the dimensions and the period of the microstructure because of the increasing computational requirements. In order to observe the optical field in the focal region experimentally, we analyse two-dimensional arrays of approximately hemispherical microlenses illuminated with a plane wave. For the simulation we perform two-dimensional calculations (transverse electric polarization). Three-dimensional calculations are not possible because of the computational requirements, which exceed by far the available capacities. For the two-dimensional calculations we use a periodic line of infinitely long cylindrical lenses [18] and we represent the lens surface as part of a perfect circle, which does not completely correspond to a real microlens fabricated by the resist melting technology, but is a good approximation for the microlenses studied. The precise form of a microlens and, hence, also its focal properties are determined by the effects of surface tension, temperature and the rate and manner of the temperature change during fabrication [19].

The microlenses presented have a diameter of $d = 30$ μm, a height of $h = 10$ μm and a focal length of $f \approx 35$ μm (NA $\approx$ 0.4). The 2D array period is 33 μm. In figure 7(a) we present the measured intensity distribution. The lens is illuminated with a plane wave propagating in the z-direction (in the figure from top to bottom). The intensity distribution in the focal region is strongly modulated by diffraction due to the high numerical aperture. Comparing with the calculated

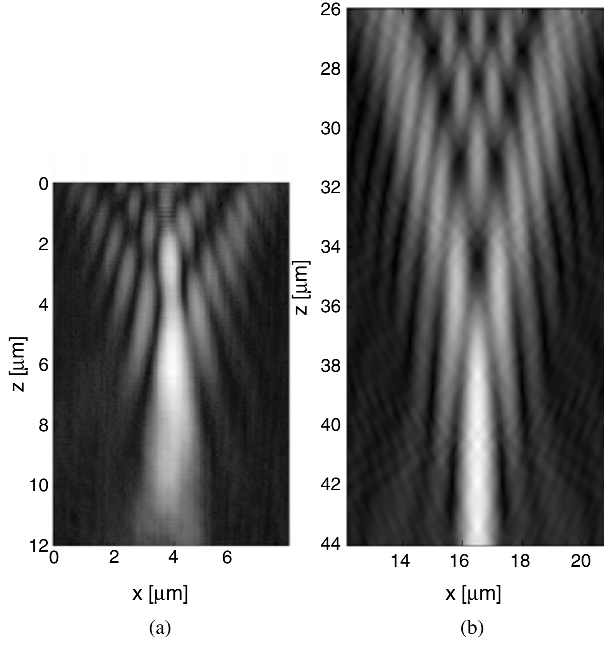

Figure 7. The intensity distribution in the focal region of a microlens ($d = 30\ \mu$m, $f \approx 35\ \mu$m). (a) Measured with the HRIM ($\Delta z = 50$ nm: defined by the step size of the piezo-stage, $\Delta x = 35$ nm: pixel size in the object field). The slight asymmetry may be due to a misalignment of the illumination. $z = 0$ indicates the starting plane of the measurements. Due to experimental limitations, the absolute distance between the starting plane and the lens is not known. (b) Calculated with the rigorous modal method (FMM). The z-axis represents the distance to the microlens.

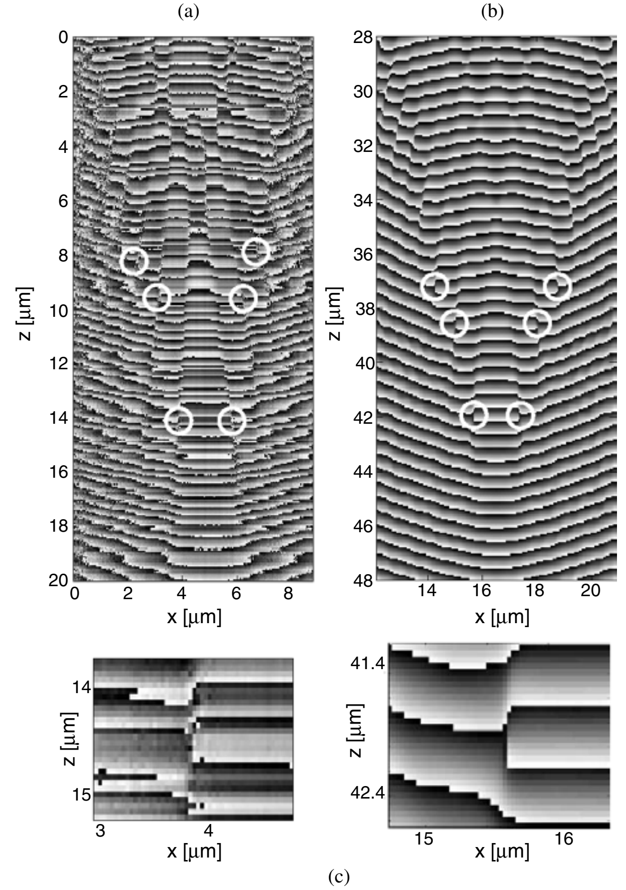

Figure 8. The phase distribution in the focal region of a microlens ($d = 30\ \mu$m, $f \approx 35\ \mu$m). The greyscale range is between π (white) and $-\pi$ (black). (a) Measured with the HRIM ($\Delta z = 50$ nm: defined by the step size of the piezo-stage, $\Delta x = 35$ nm: pixel size in the object field). $z = 0$ indicates the starting plane of the measurements. Due to experimental limitations, the absolute distance between the starting plane and the lens is not known. (b) Calculated with the rigorous modal method (FMM). The z-axis represents the distance to the microlens. (c) Enlargement of an encircled region containing one singularity (lower left singularity in figures 3(a) and (b)).

intensity, shown in figure 7(b), and considering the differences between the 2D model and 3D lens, we observe a good correspondence in the diffraction pattern. However, we notice that the calculated intensity is stretched in the z-direction in comparison with the measured intensity. Further, in the calculated diffraction pattern we observe a dark region just above the focus, which is not present in the measurements. This may be due to the fact that the calculations generate a two-dimensional pattern whereas the measurements refer to a section of an axially symmetric 3D diffraction pattern [20]. Variations may also be caused by the difference between the shape of the real microlens and the shape of the simulated microlens. The diffraction contributions of the neighbouring lenses cannot be noticed because most of the energy is diffracted into lower orders [18].

The behaviour of the phase in the focal region of the microlenses is illustrated in figure 8. The illumination of the microlens is again in the direction of the z-axis. The agreement between the measured (figure 8(a)) and the calculated (figure 8(b)) phase distributions allows good comparison, including the phase singularities (marked by circles). The noise in the measurements is due to the rapid changes of the intensity with position and the low intensities in regions outside the focus. There is also a contribution from relative movements caused by external influences during the measurements. Approaching the focal region from the bottom towards the lens ($z \geqslant 15\ \mu$m in the measured and $z \geqslant 43\ \mu$m in the calculated phase distribution) the wavefronts are more smoothly curved than between the focus and the lens. In general, the closer to the microlens we get (going towards $z = 0\ \mu$m), the more turbulent the wavefront is. Further, we observe that the wavefront changes the direction of its curvature starting at the centre of focus and growing progressively while approaching the microlens. This change of curvature direction starts at a specific point, which is situated between the first two phase singularities when approaching the focal region from the bottom. In a restricted region between these two singularities we can observe a planar wavefront. Additional singularities are encountered approaching further towards the microlens. They always occur in pairs in order to conserve the topology of the optical field [20].

One of the essential properties of a phase singularity in a two-dimensional section as presented in figure 8(c) is given by a phase change on a closed path around the singularity [20]:

$$\oint \mathrm{d}\varphi = \pm 2\pi. \tag{1}$$

The total phase change of $\pm 2\pi$ remains unchanged if the closed path around the singularity is varied. By using the

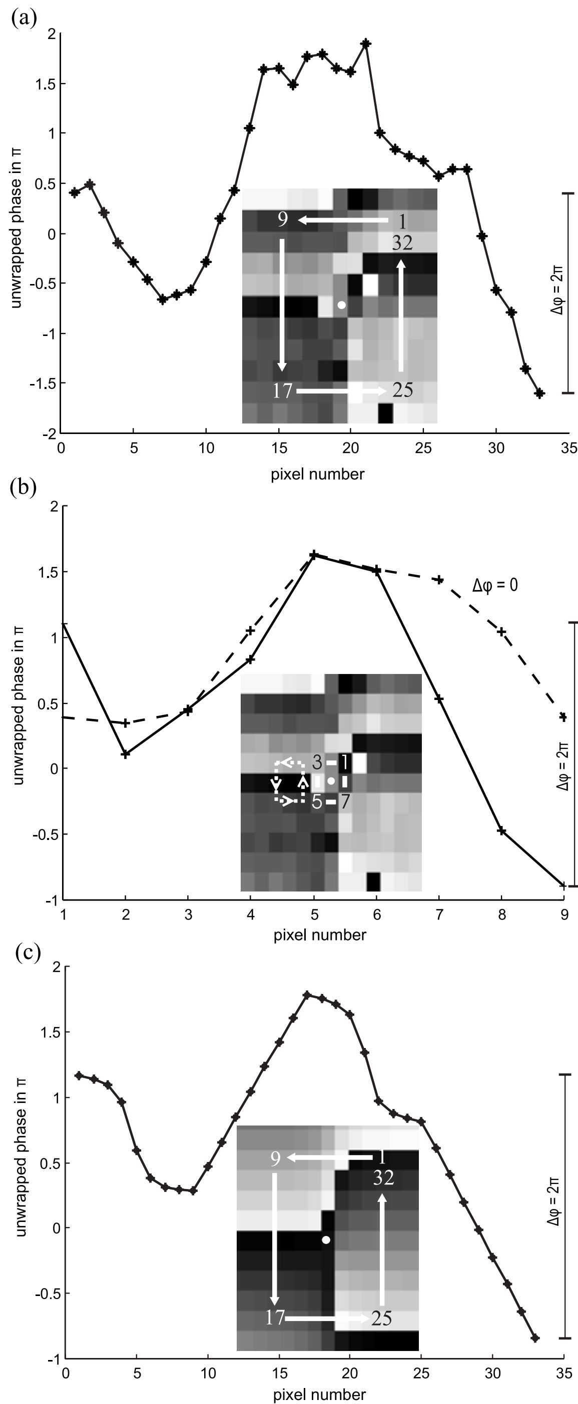

Figure 9. (a) The unwrapped phase on a closed path of 315 nm × 450 nm around the measured singularity shown in figure 8(c). (b) The unwrapped phase (solid line) on a closed path of 105 nm × 150 nm around the measured singularity shown in figure 8(c). On the same graph, the unwrapped phase (dashed line) of a laterally shifted (by 105 nm) contour not enclosing the singularity is included. In this case the phase change yields zero. (c) The unwrapped phase on a closed path of 315 nm × 450 nm around the singularity in the simulated field shown in figure 8(c). The insets show the path in the phase distribution. The values shown on the graph can vary by a multiple of 2π in comparison with the convention used in figure 8 due to the unwrapping of the phase.

measurements, we calculate the phase on the path around the singularity. To prevent adjacent pixels from acquiring

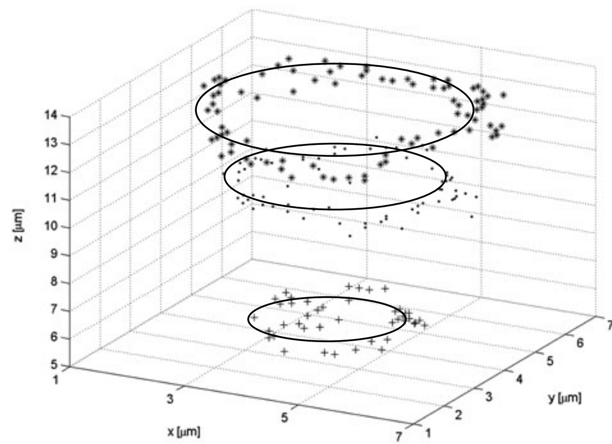

Figure 10. Singularity positions extracted from the 3D measurements for a microlens without astigmatism.

a difference in phase that exceeds π, phase unwrapping is used [21]. Figures 9(a) and (b) show the unwrapped phase on two different paths around the measured singularity of figure 8(c) with the corresponding phase change of 2π. This property allows us to localize the singularity to within the region of 105 by 150 nm (figure 9(b)), which is less than the diffraction limit. To confirm the accuracy of locating the singularity, an additional curve (dashed line) is added to figure 9(b), showing the unwrapped phase on a closed path (laterally shifted by 105 nm) not enclosing the singularity. Figure 9(c) shows the unwrapped phase on a path equivalent to the one in figure 9(a) around the singularity in the simulated field shown in figure 8(c). A good comparison between figures 9(a) and (c) can be drawn. Notwithstanding the present noise in the measured phase distribution due to low intensity in the vicinity of singularities, we are able to localize the phase singularity with subwavelength accuracy.

It is interesting to note that the observed intensity diffraction pattern in figure 7 is most similar to the Pearcey pattern [20]. However, the measured and calculated phase distributions show a different behaviour inside the caustics. The Pearcey pattern presents pairs of singularities inside the caustics whereas we cannot observe such in the rigorously calculated intensity distribution. The measured phase distribution may contain singularities inside the caustics (for $z < 8$ μm), but they are not discernible with assurance due to the present noise. In addition, our calculations have shown that singularities inside the caustics are only present for lenses of significantly greater size than the ones studied in this paper. This finding is in accordance with recently published investigations by Nye [23].

Next, we investigated the measured phase singularities in three-dimensional space. In general, dislocations are curved lines in space. By scanning through the 3D measurements the positions of different pairs of singularity have been extracted. Enough singularity positions have been extracted to indicate the form of the dislocation lines. The phase singularities are situated on different concentric circles (figure 10) forming circle dislocations according the Airy pattern, and because they are perpendicular to the direction of propagation they are of pure edge type [20].

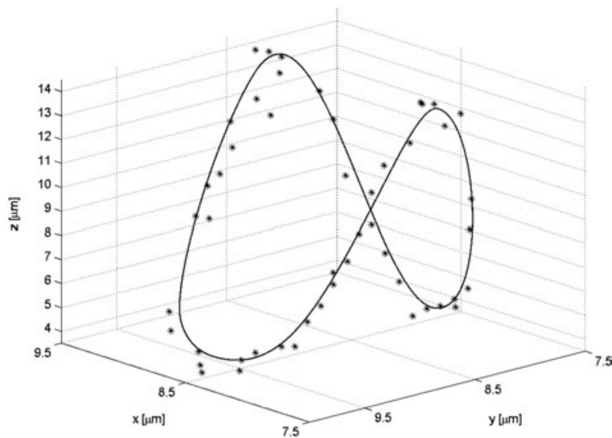

Figure 11. Singularity positions extracted from the 3D measurements for a microlens with astigmatic aberrations.

The fact that the measured dislocations are circles perpendicular to the direction of propagation indicates that the microlens investigated has no serious astigmatic aberrations. In the presence of astigmatism, the dislocation circles are distorted out of the plane perpendicular to the optical axis. An example of such a distorted dislocation from a different microlens is presented in figure 11. The extracted singularity points forming the dislocation line are no longer situated in a plane perpendicular to the direction of propagation. This observation indicates astigmatic aberration for the microlens investigated. By observing dislocation lines in the focal region, we get information about the quality of the focal properties, which are key attributes in applications of microlenses.

6. Conclusion

We have presented two different instruments for phase measurements of optical fields with subwavelength resolution: a heterodyne scanning probe microscope (heterodyne SNOM) and a high resolution interference microscope (HRIM). In particular, we have used them to determine the existence and properties of phase singularities. For both instruments we have demonstrated subwavelength resolution for the phase measurements with a spatial sampling of the order of 10 nm and a corresponding resolution for the position of the phase singularities.

Using the heterodyne SNOM we were able to measure the phase around two adjacent phase singularities separated by less than 300 nm at a wavelength of $\lambda = 532$ nm. We have also verified that the phase turns around these two phase singularities in opposite directions, which means that they have opposite topological charge, as expected by theory.

By means of high resolution interference microscopy we have been able to image the intensity and the phase distribution in the focal region of microlenses. There is a good qualitative agreement between the measured optical intensity and phase distribution and the results of rigorous diffraction theory applied to a two-dimensional model. We have been able to observe the predicted phase singularities in the measurements. They are situated in the focal region and define characteristic points where the wavefront curvature changes its direction. Closer three-dimensional investigations of the phase distribution in the focal region show that phase singularities form closed lines in space in order to conserve the optical field topology. This confirms the presence of dislocation rings corresponding to the Airy ring in a focal pattern. The measurements for an astigmatic microlens show that the dislocation line is distorted along the optical axis indicating the aberrations of this focusing microlens.

Comparing the two instruments, there is a significant difference concerning the vectorial aspect of the detected electric field: in the case of the high resolution interference microscope the non-paraxial field (large numerical aperture) produced by a microscopic object is transformed into a paraxial field at the observation plane of the microscope; therefore the electric field has only transverse components and the detected polarization is selected by the polarization of the reference wave, whereas the heterodyne SNOM probes directly the non-paraxial field with transverse and longitudinal components of the electric field vector [22]. In this latter case, the detected signal depends on the field conversion (vectorial transfer function of the tip) and the propagating mode in the fibre probe.

References

[1] Nesci A, Dändliker R and Herzig H P 2001 Measuring amplitude and phase distribution of fields generated by gratings with sub-wavelength resolution *Opt. Lett.* **26** 208–10

[2] Dändliker R, Blattner P, Rockstuhl C and Herzig H P 2001 Phase singularities generated by optical microstructures: theory and experimental results *Proc. SPIE* **4403** 257–61

[3] Nesci A, Dändliker R, Salt M and Herzig H P 2002 Measuring amplitude and phase distribution of fields generated by gratings with sub-wavelength resolution *Opt. Commun.* **205** 229–38

[4] Nye J F and Berry M V 1974 Dislocations in wave trains *Proc. R. Soc.* A **336** 165–90

[5] Vaccaro L, Nesci A, Dändliker R and Herzig H P 2002 Heterodyne scanning near-field optical microscope *Proc. SPIE* **4829** 637–8

[6] Hariharan P, Oreb B F and Eiju T 1987 Digital phase-shifting interferometry: a simple error-compensating phase calculation algorithm *Appl. Opt.* **26** 2504

[7] Tychinski V P 1989 On superresolution of phase objects *Opt. Commun.* **74** 41–5

[8] Totzeck M and Tiziani H J 1995 Interference microscopy of sub-lambda structures: a rigorous computation method and measurements *Opt. Commun.* **136** 61–74

[9] Totzeck M and Tiziani H J 1997 Phase singularities in 2D diffraction fields and interference microscopy *Opt. Commun.* **138** 365–82

[10] Brenner K-H and Singer W 1993 Light propagation through microlenses: a new simulation method *Appl. Opt.* **32** 26

[11] Wang A and Prata A 1995 Lenslet analysis by rigorous vector diffraction theory *J. Opt. Soc. Am.* A **12** 1161

[12] Walford J N, Nugent K A, Roberts A and Scholten R E 2002 High-resolution phase imaging of phase singularities in the focal region of a lens *Opt. Lett.* **27** 5

[13] Karman G P, Beijersbergen M W, van Duijl A and Woerdman J P 1997 Creation and annihilation of phase singularities in a focal field *Opt. Lett.* **22** 19

[14] Nye J F 1991 Diffraction by a small unstopped lens *J. Mod. Opt.* **38** 743–54

[15] Karman G P *et al* 1998 Airy pattern reorganization and subwavelength structure in a focus *J. Opt. Soc. Am.* A **15** 884–99

[16] Turunen J 1997 Diffraction theory of microrelief gratings *Micro Optics* ed H P Herzig (London: Taylor and Francis) pp 31–52

[17] Hutley M C 1997 Refractive lenslet arrays *Micro Optics* ed H P Herzig (London: Taylor and Francis) pp 127–52

[18] Blatter P and Herzig H P 1998 Rigorous diffraction theory applied to microlenses *J. Mod. Opt.* **45** 1395–403

[19] Schilling A, Merz R, Ossman Ch and Herzig H P 2000 Surface profiles of reflow microlenses under the influence of surface tension and gravity *Opt. Eng.* **39** 2171–6

[20] Nye J F 1999 *Natural Focusing and Fine Structure of Light, Caustics and Wave Dislocations* (Bristol: Institute of Physics Publishing)

[21] Huntley J M 1989 Noise immune phase unwrapping algorithm *Appl. Opt.* **28** 3268–70

[22] Nye J F and Hajnal J V 1987 The wave structure of monochromatic electromagnetic radiation *Proc. R. Soc.* A **409** 21–36

[23] Nye J F 2003 Evolution from a Frauenhofer to a Pearcey diffraction pattern *J. Opt. A: Pure Appl. Opt.* **5** 495–502